Comparison of Coding Capabilities of Type I and Type II Neurons

MARTIN ST-HILAIRE AND ANDRÉ LONGTIN
Department of Physics, University of Ottawa, 150 Louis Pasteur, Ottawa, Ontario, Canada, K1N 6N5

Action Editor: G. Bard Ermentrout

Abstract. We consider the dependence of information transfer by neurons on the Type I vs. Type II classification of their dynamics. Our computational study is based on Type I and II implementations of the Morris-Lecar model. It mainly concerns neurons, such as those in the auditory or electrosensory system, which encode band-limited amplitude modulations of a periodic carrier signal, and which fire at random cycles yet preferred phases of this carrier. We first show that the Morris-Lecar model with additive broadband noise ("synaptic noise") can exhibit such firing patterns with either Type I or II dynamics, with or without amplitude modulations of the carrier. We then compare the encoding of band-limited random amplitude modulations for both dynamical types. The comparison relies on a parameter calibration that closely matches firing rates for both models across a range of parameters. In the absence of synaptic noise, Type I performs slightly better than Type II, and its performance is optimal for perithreshold signals. However, Type II performs well over a slightly larger range of inputs, and this range lies mostly in the subthreshold region. Further, Type II performs marginally better than Type I when synaptic noise, which yields more realistic baseline firing patterns, is present in both models. These results are discussed in terms of the tuning and phase locking properties of the models with deterministic and stochastic inputs.

Keywords: neural coding, information theory, Type I neuron, Type II neuron, Morris Lecar model, phase locking, noise, electric fish, bifurcation theory

1. Introduction

One possible classification of neurons is based on their behavior as they go from quiescence to periodic firing of action potentials (Hodgkin, 1948; Rinzel and Ermentrout, 1991). For Type I neurons, this transition is characterized by a saddle-node bifurcation on an invariant circle. For this bifurcation (which we will henceforth refer to as "saddle-node" or Type I for brevity), the firing frequency is zero at the bifurcation, and increases smoothly with bias current from this point on. The corresponding bifurcation for Type II neurons is of the Andronov-Hopf type (which we will refer to as Hopf or Type II for short). In this latter case, the onset of firing occurs with an abrupt jump from zero to a finite frequency at the bifurcation, and the frequency

increases smoothly with bias current thereafter. Type I and II neurons also differ from the point of view of other dynamical properties such as response latencies and frequency tuning. For example, it has been suggested that Type I neurons act as integrators of incoming signals, since input spikes work together best to produce firing when they are in close temporal succession. In contrast, Type II neurons behave more like resonators, in the sense that they tend to fire when driven near a certain resonant frequency (Izhikevich, 2001).

It is not known what the relative merits of the Type I and Type II behaviors are with respect to the encoding of general aperiodic time-varying stimuli. Further, neurons often operate in the presence of a significant amount of noise of synaptic origin. This further

complicates the analysis of the relative merits of Type I versus Type II coding. In this paper, we investigate these questions computationally in a common situation: the encoding of amplitude modulations of a carrier wave into spike trains in Type I and Type II neurons, with and without synaptic noise.

Many neurons must encode amplitude variations of a periodic carrier signal (Carr and Friedman, 1999). This is true in particular for neurons in the auditory and electrosensory systems (Gabbiani, 1996a,b; Machens et al., 2001). It has long been known that periodic forcing can lead to various forms of phase locked behavior (French et al., 1972; Knight, 1972; Keener et al., 1981). Primary auditory receptors in many species respond to a pure tone by firing near a preferred phase but at more or less random cycles of this carrier (Rose et al., 1967; Kiang et al., 1964). Hereafter we refer to this pattern as "skipping". The probability of firing on a given cycle is usually proportional to the instantaneous amplitude of the carrier. Hence, a time-varying stimulus produces a time-varying carrier amplitude, which is encoded by the neuron as changes in the rate of firing of phase locked spikes. We are ultimately interested in understanding the membrane properties underlying such encoding processes and which are at work in a variety of senses across many species.

Such firing activity also occurs in the encoding of vibratory stimuli (Talbot and Mountcastle, 1969), and in weakly electric fish that probe their environment via active electrolocation and electrocommunication (see Turner et al., 1999; Bastian, 1994 for reviews). We describe this sense in more detail here since it has the main features of carrier-based encoding and since it is the prime motivation for our work.

A weakly electric fish emits a periodic electric field known as the electric organ discharge (EOD). Along the surface of its skin, this carrier induces a periodic transdermal potential. "P-unit"-type receptors ("P" for "probability coders") exhibit skipping in response to this forcing (Scheich et al., 1973; Wessel et al., 1996). Each electroreceptor has its own mean probability P of firing at each EOD cycle (typically $0.1 < P < 0.6$). This P value usually refers to the mean probability in the absence of stimulus, which in the case of active electrolocation corresponds to the unmodulated quasi-sinusoidal EOD alone. For an auditory system, the P-value would depend on the amplitude of an unmodulated pure tone stimulus. The precise role of the P value in information transfer is not known, although generally more information seems to be conveyed for higher values of P (Wessel et al., 1996; Longtin and St-Hilaire, 2000).

The EOD is perturbed by nearby objects with an impedance different from that of the surrounding water (Bastian, 1994). This results mainly in an amplitude modulation (AM) of the EOD carrier. Since the spike rate of a P-unit depends on the EOD amplitude, its instantaneous firing rate is modified by the AM. The P value is a smoothly increasing function of the EOD amplitude in e.g. Eigenmannia (Scheich et al., 1973) and in Apteronotus Leptorhynchus (Wessel et al., 1996; Nelson et al., 1997), as it is in auditory afferents (Rose et al., 1967).

Various combinations of excitability with deterministic and stochastic driving can produce skipping behavior in a variety of neural models, such as ionic models or reduced versions such as the leaky integrate-and-fire or FitzHugh-Nagumo model (see e.g. Longtin, 2002 for a review). While it is possible to obtain such behavior without noise (the solution is then chaotic), the behavior is more robust with noise, i.e. it persists over a range of stimulation parameters. Given that spontaneous release of neurotransmitter is known to occur between receptor cells and afferent nerves, it is justified to investigate skipping generated by noisy excitable dynamics. It has also been shown (Longtin, 1995) that the Morris-Lecar model with Type II dynamics, sinusoidal forcing and additive noise can produce skipping. Below we find that this is also the case for Type I, and that both Types can exhibit a monotonic increase of P with carrier amplitude. Noise further smoothes out this relationship. Our goal here is not to provide detailed fits to specific data; this is done e.g. in Chacron et al. (2000) using a leaky integrate and fire model with dynamical threshold. Rather, we wish to show that the dominant phase locked features of the data can be reproduced in the Morris-Lecar model.

Given this correspondence of the model behaviors with the data in the absence of AM's, our work goes on to address how internal synaptic noise affects the process of encoding bandlimited AM's. Noise has been incorporated into neuronal models for many decades now (see e.g. Geisler and Goldberg, 1966 in the case of primary auditory fibers). Although intracellular recordings from P-type electroreceptors are not yet possible, it is strongly believed that synaptic transmission, in particular the fluctuating number of release sites and their unreliability, underlies much of the noisy component of the encoding process

in these receptors (Xu et al., 1996; Chacron et al., 2000).

It is known (Rinzel and Ermentrout, 1999) that Type II dynamics have more resonant properties, and may perhaps be best at firing near certain frequencies rather than smoothly encoding time-varying signals (Longtin and St-Hilaire, 2000; Izhikevich, 2001; Masuda and Aihara, 2002). On the other hand, Type I dynamics have significant response latencies, despite a continuous f-I characteristic. It is not obvious a priori which Type would best convey information about time-varying stimuli. The answer may depend on the frequency content of the input as well as on the carrier frequency.

Here we begin investigating this multifaceted problem by focussing on a specific input, namely low frequency band-limited Gaussian noise causing amplitude modulations of a fixed-frequency carrier. The coding portion of our study considers the effect of distance-to-threshold and synaptic noise on information transfer in Type I and II implementations of the Morris-Lecar model.

The paper is organized as follows. Section 2 presents the models under study and details the methods used for simulations and "quality of encoding" calculations. Section 3 studies deterministic and stochastic phase locking and tuning properties for both model Types. The matching of the firing rates of both models for information transfer comparisons is performed in Section 4. The encoding of AM's in both models with the calibration of Section 4, as well as a comparison of coding in both models, is the subject of Section 5. The paper ends in Section 6 with a discussion of the results in the light of the known properties of Type I and II neurons.

2. Methods

2.1. Model

The model developed by Morris and Lecar (ML) was first used in the study of the barnacle muscle fiber. It involves two voltage-gated ionic currents, a Ca^{2+} channel and a K^+ channel:

$$C\dot{v} = -g_{Ca}m_\infty(v)(v - V_{Ca}) - g_K w(v - V_K)$$
$$\qquad - g_L(v - V_L) + I_{EOD} + I \qquad (1)$$
$$\dot{w} = \phi \frac{[w_\infty(v) - w]}{\tau_w(v)} \qquad (2)$$

where

$$m_\infty(v) = \frac{1}{2}\left[1 + \tanh\left(\frac{v - V_1}{V_2}\right)\right] \qquad (3)$$

$$w_\infty(v) = \frac{1}{2}\left[1 + \tanh\left(\frac{v - V_3}{V_4}\right)\right] \qquad (4)$$

$$\tau_w(v) = 1/\cosh\left(\frac{v - V_3}{2V_4}\right) \qquad (5)$$

Here v is the voltage variable, w and m represent the fraction of open channels for K^+ and Ca^{2+}, respectively, and the infinity subscript indicates the pseudo-steady state of the variable. The time scale of m being much more rapid than that of the voltage, the model assumes that m always reaches its pseudo-steady state value (m_∞) instantaneously. ϕ is a prefactor that accounts for temperature-like effects (ϕ is kept constant in our study), and I is the bias current. The voltage variable here is also forced additively with the post-synaptic current I_{EOD} resulting from the amplitude-modulated carrier, hereafter referred to as the EOD (see Introduction):

$$I_{EOD} = r_0[1 + s(t) + \eta(t)]\sin(\beta t) \qquad (6)$$

where r_0 is the mean EOD amplitude, and $s(t)$ is the band-limited random amplitude modulation (RAM); the standard deviation of this noise is kept constant throughout our study, and set equal to 17% of the EOD amplitude as in Wessel et al. (1996). η is synaptic noise, modeled simply as an Ornstein-Uhlenbeck process with correlation time (i.e. inverse bandwidth) τ_{OU}:

$$\tau_{ou}\frac{d\eta}{dt} = -\eta + \xi_1(t) \qquad (7)$$

where $\xi_1(t)$ is zero-mean Gaussian white noise with autocorrelation $\langle\xi_1(t)\xi_1(t')\rangle = 2D\delta(t - t')$. *Hereafter we refer to the synaptic noise intensity as D.* A simple multiplicative coupling of η to r_0 is assumed here (Chacron et al., 2000), meaning that the noise level is proportional to the mean amplitude of the EOD, a reasonable property for the sum of point processes that constitute the synaptic events.

The choice of model parameters in Table 1 was based on Rinzel and Ermentrout (1991); our Type I and II parameters are identical to theirs, except that v_3 and v_4 slightly differ for the Type II case. The input stimulus

Table 1. Morris-Lecar parameters for the Type I and Type I implementations used in our study.

Parameter	Type II	Type I
V_1	−0.01	−0.01
V_2	0.15	0.15
V_3	0.0167	0.1
V_4	0.25	0.145
V_{Ca}	1.7	1.0
V_K	−0.7	−0.7
V_L	−0.5	−0.5
g_{Ca}	1.1	1.0
g_K	2.0	2.0
g_L	0.5	0.5
C	1.0	1.0
ϕ	0.2	0.333
τ_{ou}	0.025	0.025

$s(t)$, i.e. the RAM, was generated by filtering Gaussian white noise with a fourth-order low-pass filter:

$$\frac{ds}{dt} = z_1 \tag{8}$$

$$\frac{dz_1}{dt} = z_2 \tag{9}$$

$$\frac{dz_2}{dt} = z_3 \tag{10}$$

$$\frac{dz_3}{dt} = -4\alpha z_3 - 6\alpha^2 z_2 - 4\alpha^3 z_1 - \alpha^4 s + \xi_2(t) \tag{11}$$

where ξ_2 is a second independent Gaussian white noise. A refractory period check is implemented numerically to prevent fast-varying input from generating firing events that are too close in time, thus mimicking the observed refractoriness in actual P-units (they never fire more than once per EOD period). Each simulation spanned 2×10^7 time steps, in which the first 10^5 steps were discarded as transients. A fixed time step Euler-Maruyama stochastic integration scheme (Fox et al., 1988) was used with step size $dt = 0.025$ ms.

Typical voltage time series of the Morris-Lecar model in response to random amplitude modulations of the EOD are shown in Fig. 1 for the Type I and II cases in the subthreshold regime, and in Fig. 2 for the suprathreshold regime. Note that for both these figures, there is no internal synaptic noise, only RAM's. Internal noise simply produces jitter and missed cycles or
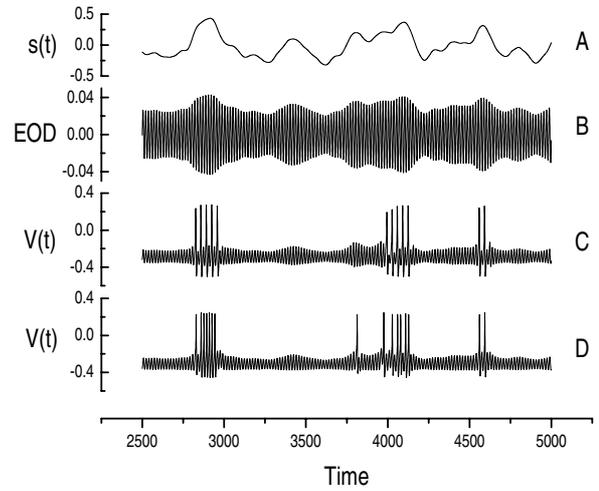

Figure 1. Time series of (A) the stimulus envelope (i.e. the RAM), (B) the EOD waveform, (C) the voltage for the Type I parameters and $I = 0.0718$, and (D) the voltage for the Type II parameters and $I = 0.135$. There is no synaptic noise. All other parameters are as per Table 1. For both types, this corresponds to a subthreshold regime in the presence of periodic forcing of amplitude $r_0 = 0.03$ and frequency $\beta/(2\pi) = 60$ Hz. Subthreshold here means that, in the absence of random amplitude modulations but in the presence of the periodic EOD, no firings can occur; the firings seen are thus a result of the AM. The boundary between these subthreshold and suprathreshold behaviors (see Fig. 2) depends on the frequency and amplitude of the EOD forcing. Note that the whole time scale of the dynamics can be adjusted simply by rescaling time to match the EOD frequency of a particular fish. For example, for the species Apteronotus Leptorhynchus, the EOD frequency can vary across specimens in the range of 600 to 1000 Hz. All simulations in our paper use an EOD frequency of 60 Hz, and the cutoff frequency of the random amplitude modulations is 6 Hz. It is straigthforward then to scale our results for a specific EOD frequency of choice.

extra firings on cycles that would otherwise not have produced a spike.

2.2. Numerics

A Matlab routine (Gabbiani and Koch, 2000) was adapted for information measurements on the simulation results from each model. The routine computes an optimal linear filter $h(t)$ that yields the best linear estimate (in the mean square sense) $s_{est}(t)$ of a signal $s(t)$ given the observed output spike train $x(t)$ (the mean values are subtracted from $s_{est}(t)$, $s(t)$ and $x(t)$):
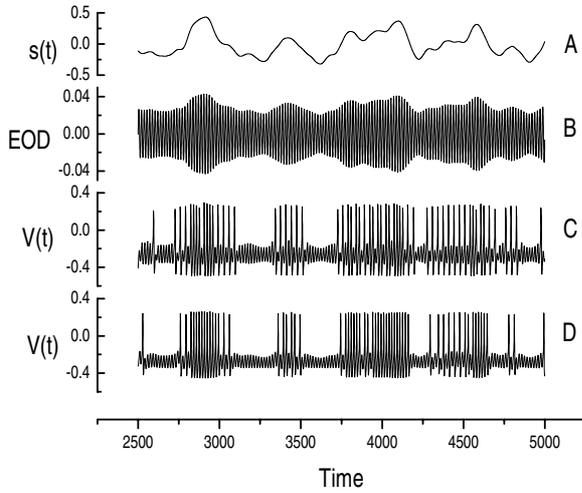
$$x(t) = \sum_i \delta(t - t_i) - x_0 \tag{12}$$

Figure 2. Time series of (A) the stimulus envelope (i.e. the RAM), (B) the EOD waveform, (C) the voltage for the Type I parameters and $I = 0.0763$, and (D) the voltage for the Type II parameters and $I = 0.149$. There is no synaptic noise. All other parameters are as per Table 1. For both types, this corresponds to a suprathreshold regime in the presence of periodic forcing of amplitude $r_0 = 0.03$ and frequency $\beta/(2\pi) = 60$ Hz. Suprathreshold here means that, in the absence of random amplitude modulations but in the presence of the periodic EOD, firings can occur (and do so in some periodic phase locked pattern).

where x_0 is the mean firing rate. The stimulus reconstruction method yields $s_{\text{est}}(t)$ by convolving the spike train with the optimal filter $h(t)$

$$s_{\text{est}}(t) = \int_0^T dt' h(t - t') x(t'), \qquad (13)$$

where T is the total duration of the spike train. The filter is chosen so that the mean square error associated with the estimate,

$$\epsilon^2 = \frac{1}{T} \int_0^T dt [s(t) - s_{\text{est}}]^2, \qquad (14)$$

is minimized. From the orthogonality principle, one finds that the expression for the filter in the frequency domain is:

$$h(f) = \frac{S_{sx}(-f)}{S_{xx}(f)} \qquad (15)$$

where $S_{sx}(f)$ and $S_{xx}(f)$ are the Fourier transforms of the cross-correlation between the stimulus and spike train R_{sx} and of the autocorrelation function of the spike train R_{xx}, respectively.

In practice, the Matlab routine first generates a spike train $x(t)$ (an array of '0's and '1's) from the inter-spike times t_i, with sample step equal to the inverse of the sampling rate of $s(t)$. The Nyquist frequency of the sampling is chosen much larger than the cutoff frequency of the bandlimited stimulus in each model to avoid aliasing. After subtraction of the respective mean values of $x(t)$ and $s(t)$, estimates of $S_{sx}(f)$ and $S_{xx}(f)$ are computed using an averaging method (from the Matlab signal processing toolbox) assuming ergodicity of the process; the power and cross-power spectral densities of Eq. (15) are averaged over windows of 2048 points (with overlap of 1024) from the spike train and stimulus. Each section of the signal is Bartlett-windowed (Press et al., 1992) before the spectral density is evaluated. All simulations contained at least 100,000 points so that nearly 100 samples were used for the calculation of a particular $h(t)$.

The coding fraction γ, a normalized measure of the quality of coding based on the quality of stimulus reconstruction, is defined as in Wessel et al. (1996):

$$\gamma = 1 - \frac{\epsilon}{\sigma}. \qquad (16)$$

It takes values between 0 (spike train is uncorrelated with the original stimulus, $\epsilon^2 = \sigma^2$) and 1 (the reconstruction is perfect, i.e. the reconstruction noise is $\epsilon = 0$).

3. Firing Characteristics

3.1. Type II

When forced by only a constant current bias term I (no carrier, i.e. $r_0 = 0$), our implementation of Type II Morris Lecar undergoes a Hopf bifurcation at a critical bias current value $I_c = 0.183$, as shown in Fig. 3. For any currents below I_c, the model converges to a rest state dependent on the actual value of the current. For currents above I_c—and up to another bifurcation value which is not of interest here—the Type II ML exhibits a periodic solution with a period of ≈ 32 ms.

When forced with a current $I < I_c$ and the constant amplitude sinusoidal term (the EOD), the Type II Morris-Lecar responds in a phase locked manner. This is shown in the devil's staircase structures in plots of P vs. the amplitude r_0 in Fig. 4 for two distinct bias current values. The P value is simply a measure of firing rate, since the EOD frequency is kept constant. The relative distances from the threshold for the two
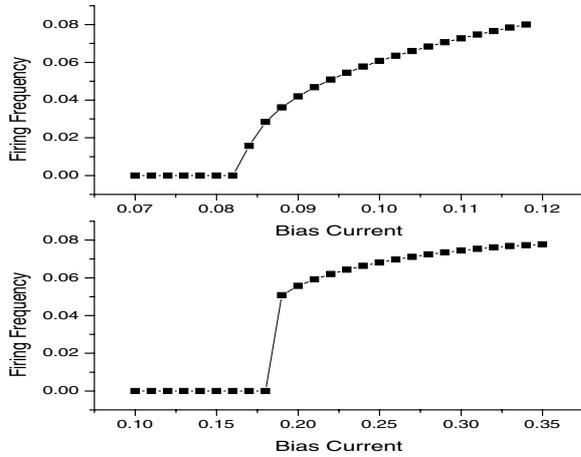
Figure 3. Mean firing rate versus bias current I in Eqs. (1) and (2) for Type I (top) and II (bottom) in the absence of synaptic noise and of an EOD (i.e. $r_0 = 0$, so that $I_{EOD} = 0$; consequently, there is also no random amplitude forcing). All other parameters are as per Table 1. These data show the boundary between subthreshold and suprathreshold behavior *as they are usually defined for excitable systems*, i.e. in the absence of all forcing (in contrast to Figs. 1 and 2 where the sinusoidal EOD is present). These boundaries (corresponding to bifurcations between quiescent and periodic firing) are $I_c = 0.083$ for Type I, and $I_c = 0.183$ for Type II. For weakly electric fish, the EOD is always present with typically the same amplitude and frequency (for a given fish), which leads to more practical definitions of "sub" and "suprathreshold" dynamics *in the presence of the EOD*, as were used in Figs. 1 and 2.

models is different here since case (A) must be forced with a greater carrier amplitude to exhibit a nonzero firing probability.

For the top panel, amplitudes less than $r_0 = 0.036$ will not produce any firing unless synaptic noise or a RAM is present. Those amplitudes are said to be *subthreshold* for this bias current. Conversely, amplitudes above $r_0 = 0.036$ are said to be *suprathreshold* as they give rise to firing without any other forcing. The equivalent threshold carrier amplitude for the bottom panel is $r_0 = 0.026$.

The large plateaus in Fig. 4 are regions of phase locking. One can easily distinguish 2:1 (1 spike in response to 2 forcing cycles), 3:1, 4:1 and even 5:1 phase lockings. Such plateaus are either smoothed out, or washed out altogether if they are small, in the presence of synaptic noise (not shown). Such noise also linearizes the output frequency-vs-I characteristic of the model shown in Fig. 3.

Phase locking is also observable in ISIHs of Type II ML (Fig. 5) for two different currents yielding two distinct regimes. We note that such patterns, along with those we will show for the Type I dynamics, exhibit many of the qualitative features seen experimentally in different units or sometimes in the same unit at different EOD amplitudes (Scheich et al., 1973;
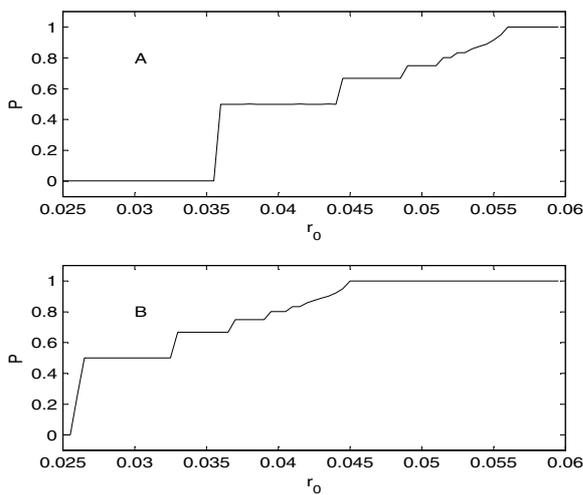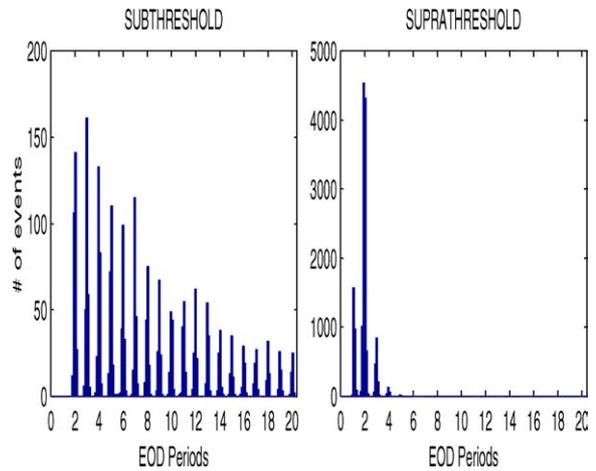

Figure 4. Probability of firing per forcing cycle as a function of the amplitude of sinusoidal forcing for the Type II Morris-Lecar system Eq. (2) without synaptic noise and random modulations of the EOD amplitude. Bias currents I are 0.135 (A) and 0.149 (B). All other parameters are as per Table 1. Note that the phase locking plateaus with $P < 0.5$ are not seen with the resolution of our computation.

Figure 5. Interspike interval histogram for the Type II Morris-Lecar model with constant amplitude periodic forcing. Both panels are obtained with $r_0 = 0.03$ and synaptic noise intensity $D = 0.06$. There is no random modulation of the EOD amplitude. The subthreshold and suprathreshold regimes are obtained using two current values of 0.135 and 0.149, for the left and right histograms, respectively. Fluctuations in mode heights are statistical; for longer simulations, the ISIH is expected to decay monotonically past the first few modes.

Wessel et al., 1996). Here both histograms were obtained with the same EOD amplitude; the subthreshold and suprathreshold regime were obtained by changing the distance to the Hopf bifurcation using the same bias current values of 0.135 and 0.149. Synaptic noise of amplitude $D = 0.06$ was also applied.

In the subthreshold regime, the model would not fire in the absence of synaptic noise. The addition of a stochastic component allows firing and the resulting gamma-distribution shape of the ISIH is typical of histograms found in mid-to-high firing rate P-units—in contrast with Gaussian-shaped histograms found for lower firing rate P-units (Scheich et al., 1973; Wessel et al., 1996). The frequency of the forcing being $f = 60$ Hz, we find clusters of intervals around multiples of $t = 16.66$ ms, equivalent to 1 EOD period.

In the suprathreshold regime, firings occur at a higher rate, hence the interspike intervals are reduced on average and the modes are shifted towards shorter intervals. In the absence of synaptic noise, this regime exhibits a 2:1 firing pattern (one spike every 2 cycles). Notice the different vertical scales, indicating a greater number of events in the suprathreshold case.

We now consider a frequency tuning curve at $I = 0.135$, shown in Fig. 6. It has the characteristic V-shape of Type II membrane, and its minimum is located slightly to the left of the period associated with its limit cycle near the onset of periodic firing ($\sim$32 ms). Notice the location of the (EOD) carrier period chosen for our study (16.6 ms) at about half the period of the limit

cycle. Because of this resonant behavior, one might expect signal transduction in Type II ML to suffer somewhat from a tendency to fire at the frequency of the intrinsic limit cycle, rather than according to the AM fluctuations of the EOD. This is expected even though the AM fluctuations are slower, ranging from 0 Hz to 6 Hz.

3.2. Type I

The critical bifurcation current for our type I model is $I_c = 0.083$ (see Fig. 3). We recall that a saddle-node bifurcation occurs at this critical value. For $I > I_c$ periodic firing emerges with zero frequency, and approximately following $f \sim (I - I_c)^{1/2}$. With periodic drive, the type I model also exhibits a devil's staircase as shown in Fig. 7 for two bias currents, 0.0718 and 0.0763. The latter values are below I_c, the (lower) first one being further away from the bifurcation. As expected, panel A reveals that a larger sinusoidal amplitude r_0 is needed to induce firing than when the system is placed closer to the bifurcation. The plateaus appear relatively smaller than for the Type II case. Also, we find that the slope of the r_0-P characteristic is steeper than for the Type II case. Thus we expect the range of EOD amplitudes that are potentially encoded by type I to be smaller. This may be unfair because of the choice of the *same* driving frequency for both type I and II. Nevertheless, we
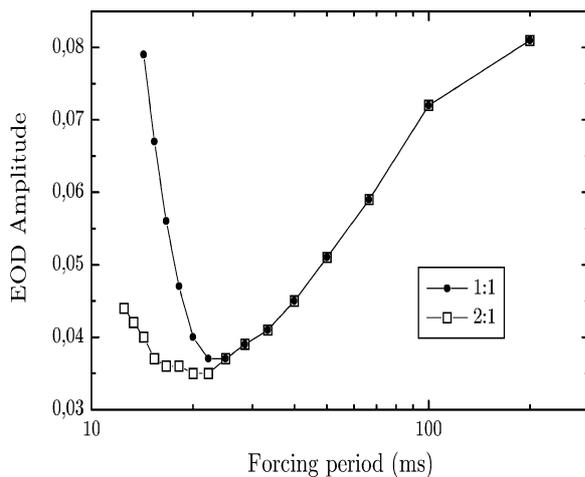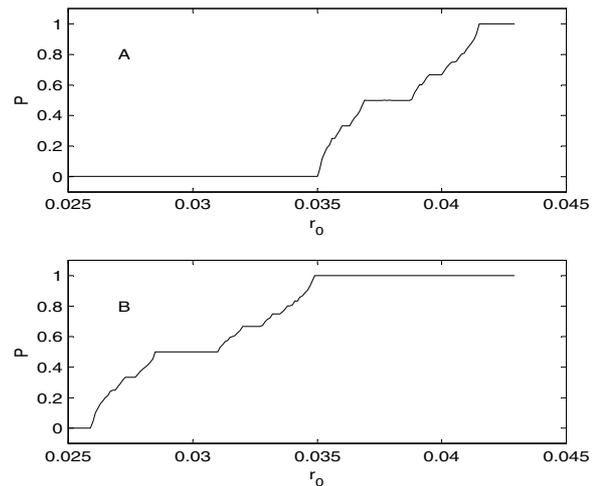
Figure 6. Tuning curve of type II Morris-Lecar. A given curve is obtained by finding, for each forcing period, the minimum amplitude giving rise to the indicated (n:m) firing pattern.

Figure 7. Probability of firing per forcing cycle as a function of the amplitude of sinusoidal forcing for the Type I Morris-Lecar system Eq. (2) without synaptic noise and random modulations of the EOD amplitude. Bias currents I are 0.0718 (A) and 0.0763 (B). All other parameters as per Table 1.
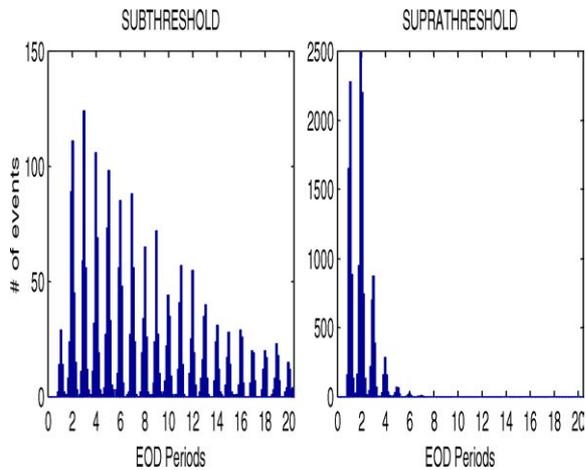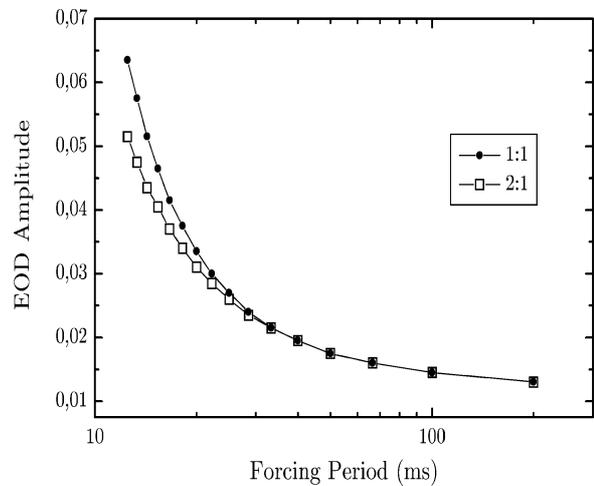
Figure 8. ISIH of the type I Morris-Lecar model with constant amplitude periodic forcing. Both panels are realized with $r_0 = 0.03$ and noise intensity $D = 0.06$. The subthreshold and suprathreshold regimes are obtained using the current values of 0.0718 and 0.0763 for the left and right histograms, respectively. Fluctuations in mode heights are statistical; for longer simulations, the ISIH is expected to decay monotonically past the first few modes.

Figure 9. Tuning curve of type I Morris-Lecar. Each curve is obtained by finding, for each forcing period, the minimum sinusoidal amplitude giving rise to the indicated (n:m) firing pattern.

have tried to compensate for this by matching the firing rates in our comparison of coding capabilities. Further, the steeper characteristic should encode minute modulations better since they induce larger changes in the firing probability per EOD cycle.

The modes in the ISIH's of Type I are slightly broader than those of Type II, although the distribution is qualitatively the same (Fig. 8). The suprathreshold case is again a perturbation of the 2:1 firing pattern, and intervals are also shifted to the left in comparison with the subthreshold case. The Type I model here allows more spikes in the first mode (ISI's of one EOD cycle) than the Type II does in both sub- and suprathreshold regimes.

The frequency-versus-input bias characteristic is continuous for the Type I models (Fig. 3), and further linearized by noise. Another important difference between both models is seen by comparing their tuning curves. The Type I tuning curve is monotonic everywhere in the range of forcing periods plotted in Fig. 9. This shape is similar to that of *P*-units (Zakon, 1986). The almost-constant and low threshold amplitude in the region of long-forcing-period (low frequency) signals suggests that slowly varying modulations should be well encoded in that type of membrane model.

This lowpass characteristic is in contrast to the "bandpass" tuning curve associated with the resonator property of the Type II model (Fig. 6), which implies that the cell will tend to fire only to inputs in a preferred frequency range (Izhikevich, 2001). However, this bandpass characteristic may not be beneficial for encoding time-varying signals, unless the coding task is to fire more or less periodically (once per forcing cycle) when a preferred frequency is present. Such coding is not likely to convey information on the continuous variations of the stimulus amplitude, and will produce a low coding fraction as defined in our study. We will see below how the Type II model can nevertheless code well such variations when their frequency content is outside of the resonance region (even though the carrier itself is near the resonance).

Our results have thus far shown similarities and contrasts in basic firing statistics of Type I and Type II models in the presence of sinusoidal forcing with and without synaptic. The results of this section clearly show that the Morris-Lecar model with sinusoidal forcing and synaptic noise, in both the Type I and II implementations, can produce skipping patterns. Although we have not shown it, skipping patterns can also arise without synaptic noise, as long as the amplitude of the sinusoidal forcing is modulated randomly in time (even if these modulations occur on a much slower time scale). The skipping then arises as a result of transients caused by the noisy modulation. However, given that the skipping is seen in the neural systems of interest when modulations are absent and present, noise is a likely component of skipping.

4. Matching Firing Probabilities

Our investigation now turns to a comparative study of the transduction of weak signals by the two Morris-Lecar models in the vicinity of their respective bifurcations. Given that information transfer is generally strongly dependent on the firing rate (see e.g. Gabbiani and Koch, 2000; Wessel et al., 1996), the comparison only makes sense if both Type I and II models exhibit similar output firing rates in response to the combined fixed-amplitude carrier, RAM and internal synaptic noise. In particular, to a first approximation, the synaptic noise can be seen as playing the role of an external stimulus; both fluctuations are in fact on equal footing in the model (see Eq. (6)). Thus, we want the responses to the EOD alone to show similar P-values over the range of synaptic noise amplitudes considered in our study. There are a number of parameters that can be varied, and it is not known which combinations of parameters (if any) can produce the desired match. For simplicity, we have chosen to perform an approximate match by tuning the bifurcation parameter I and synaptic noise intensity D for each model.

P values for both the Type II and Type I models forced with an EOD of constant amplitude 0.03 (i.e. no RAM) are plotted over the same interval of noise amplitudes in Figs. 10 and 11. Each curve is computed for
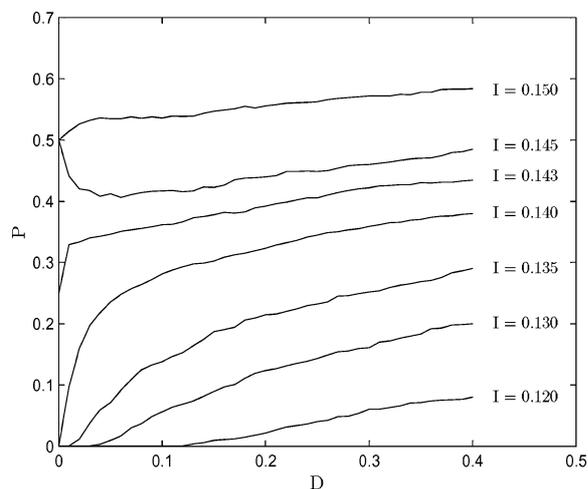

Figure 10. P vs. D for different input current values in Type II Morris-Lecar. One point was generated every $D = .001$ from the average interspike interval of a 25 sec realization. All parameters are as per Type II parameters listed in Table 1. The EOD amplitude is 0.03. Note the subthreshold curves start at $P = 0$. Also, near the boundary between sub- and suprathreshold dynamics, the internal noise initially lowers the P value, i.e. noise suppresses spikes from the limit cycle.
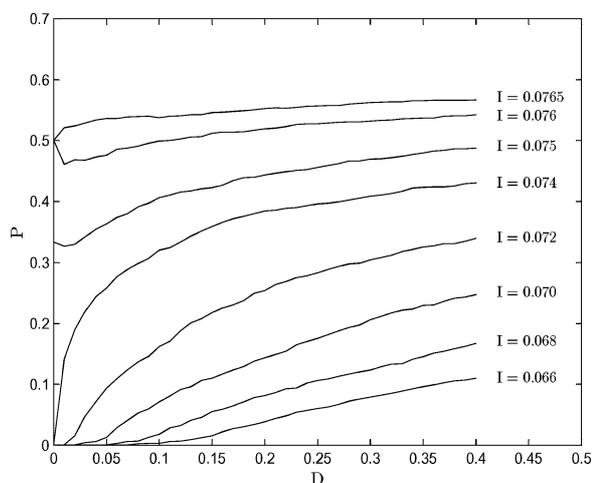

Figure 11. Firing probability per EOD cycle (P) vs. synaptic noise intensity D for different input current values for the Type I Morris-Lecar model. One point was generated every $D = .001$ from the average interspike interval of a 25 sec realization. All parameters are as per Type I parameters listed in Table 1. The EOD amplitude is 0.03. Note the subthreshold curves start at $P = 0$. As in Fig. 10, near the boundary between sub- and suprathreshold dynamics, the internal noise initially suppresses spikes from the limit cycle.

a fixed bias current. We recall that P is defined as the probability of firing per cycle without a RAM stimulus. It is expected that, for low current values, the operating point is far from the bifurcation and the resulting P value is low. Increasing synaptic noise brings the system closer to threshold and P increases. Also expected is the fact that the output rate increases as I approaches the bifurcation point.

The models were tuned so that they could be compared in both the sub- and suprathreshold regimes. For both regimes, two sets of similar P-D relations are shown in Fig. 12. They were obtained after a close investigation of Figs. 10 and 11 by generating such plots at more closely spaced current values. It was found that both models have a similar curve, in the subthreshold regime, for current values of $I = 0.0718$ (Type I) and $I = 0.135$ (Type II). Note that when the noise amplitude is zero, the P value is 0; that is why they qualify as subthreshold cases. The two curves are especially close for values of $D < 0.1$. The behavior for larger D is of lesser importance; this will become clear when comparing coding fractions, since maximal coding fractions occur in the low D region. In the suprathreshold case, current values of $I = 0.0763$ (Type I) and $I = 0.149$ (Type II) lead to very similar curves in the whole interval considered. Note that the output rate is close to
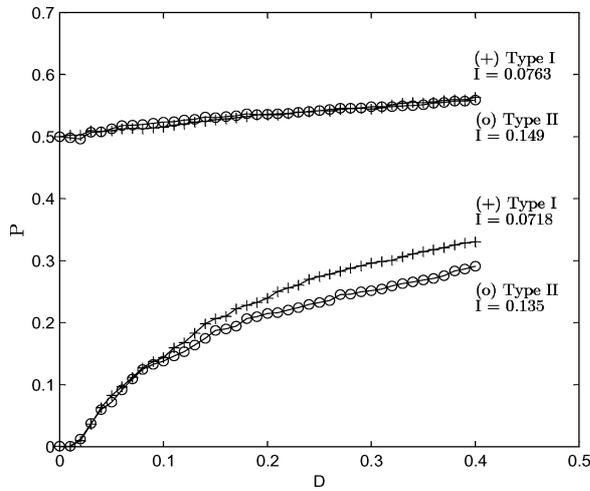
Figure 12. Comparative *P-D* curves for both subthreshold and suprathreshold cases. In all cases, there are no amplitude modulations of the EOD. Specification and parameters are as for Figs. 10 and 11. Circles (○) identify the Type II model and plus signs (+) are used for Type I. Note the close match between curves at low synaptic noise with this calibration of the two models.

constant at a fairly high value of 0.5 (far suprathreshold regime) and that the noise then has very little effect on the mean rate.

5.   Comparing Type I and II Coding Fractions

5.1.   *Effect of Internal Noise Intensity*

Using the parameters that yield closely matching *P-D* curves, we simulate the response of both models to an EOD with random amplitude modulation of standard deviation set to 17% of r_0, as in Wessel et al. (1996). One can explore the effect of many parameters on the information transfer. We will concentrate on the effect of distance to the bifurcation and the intensity of the synaptic noise. This will be done for Type I and Type II dynamics in the subthreshold and suprathreshold regimes.

Results for both models in the subthreshold regime are presented in Fig. 13 for the coding fraction as a function of the synaptic noise amplitude. Each point is obtained using the linear stimulus reconstruction technique (ref. Section 3.2). The error on each point is found by evaluating the coding fraction from multiple simulations with different initial seeds; it is on the order of ±0.01 for each point.

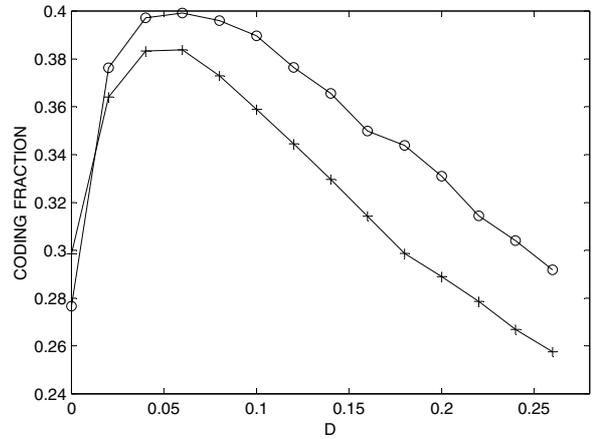Interestingly, the results for both models are very similar, although the coding fraction of Type II is ev-

Figure 13. Coding fraction vs. internal (synaptic) noise intensity in the subthreshold ML model Eq. (2). Circles (○) identify the Type II model and plus signs (+) are used for Type I. Note that these curves would be very close to one another on the (0,1) coding fraction scale. Also note how the model is able to encode signals even in the absence of internal noise; this is because the Gaussian fluctuations in the RAM sometime bring the signal above the firing threshold. Nevertheless, for $D = 0$ the model does not produce the skipping patterns seen in many neurons that encode AM's. The parameters used here match the firing rates according to Fig. 12.

erywhere slightly better than that of Type I except near the deterministic case ($D = 0$). The reconstruction quality for both models first increases from a low value with increasing noise, and goes through a maximum at roughly the same noise intensity of $D \cong 0.06$. This can be understood as follows. Low noise sometimes brings the voltage closer to threshold and raises the mean firing rate, thus the coding quality is enhanced. However, noise at intensities greater than $D \cong 0.06$ has more of a randomizing effect on the firing times (it induces useless spikes as well) and the coding fraction starts decreasing. Thus, a moderate amount of synaptic noise yields the lowest stimulus reconstruction noise, and thus the highest coding fraction; this stochastic resonance effect has been previously shown in the FitzHugh-Nagumo Type II model with random amplitude sinusoidal forcing (Longtin and St-Hilaire, 2000).

We have performed the same simulations in the suprathreshold case using bias current parameters for the matched *P-D* curves in the suprathreshold regime. Results are shown in Fig. 14. The quality of the reconstruction is seen to diminish with increasing noise intensity in both ML implementations. The error on each point is of the order of ±0.01. Here again we find that Type II is slightly better than Type I for most of the
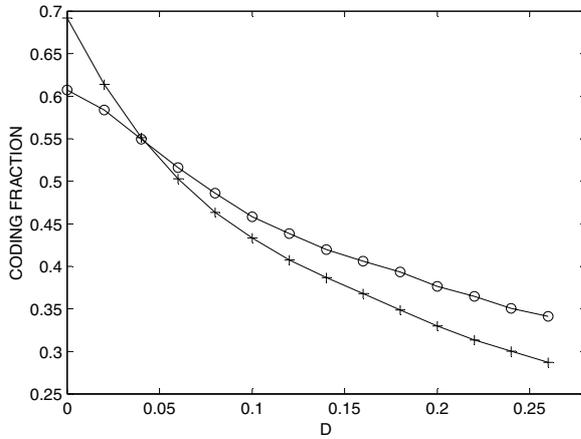
Figure 14. Coding fraction vs. noise intensity in the suprathreshold Morris-Lecar model. Circles (○) identify the Type II model and plus signs (+) are used for Type I. The parameters used match the firing rates according to Fig. 12.

range of noise intensity investigated, except at very low noise values where Type I encodes better. The Type II result here is qualitatively similar to the result from the suprathreshold (Type II) FitzHugh Nagumo model (Longtin and St-Hilaire, 2000).

5.2. Effect of Distance to Threshold

We now present results on the dependence of coding fraction γ on the distance to the bifurcation. It is not clear a priori how to quantify the "distance to a bifurcation", especially in the case of periodically driven models, as its definition is model-dependent. One might express it as the relative distance to the bifurcation, e.g. $(I - I_c) = I_c$; but in nonlinear models, this quantity is hard to relate to the driving amplitude. For example, resonance effects in the Type II model reduce the effective distance to threshold, and consequently our two models will not exhibit the same firing rates in response to the same EOD.

An attempt at comparing the distance to threshold in the context of coefficient of variation calculations is given in Gutkin and Ermentrout (1998), where the distance is simply defined as the absolute distance to the threshold (e.g. $I - I_c$). We have used both this definition and the one for relative distance given above. We present the effect of the distance to threshold on the coding fraction in Figs. 15 and 16. Results were obtained from simulations over a range of bias current values (with all other parameters constant) and plotted
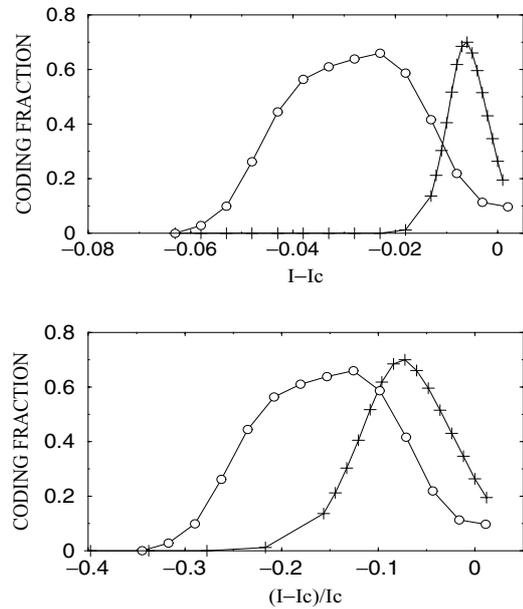

Figure 15. Coding fraction vs. absolute (upper panel) and relative (lower panel) distance to the bifurcation, without synaptic noise ($D = 0$). Circles (○) identify the Type II model and plus signs (+) are used for Type I. Threshold effects are responsible for the coding fractions going to zero at low biases, and saturation effects cause the coding fractions to go to zero at high biases. The same sampling intervals and same spike train lengths were used for each model.
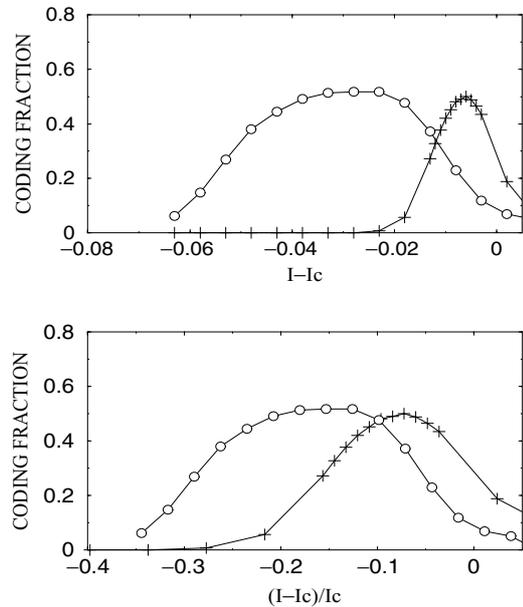

Figure 16. Coding fraction vs. absolute (upper panel) and relative (lower panel) distance to bifurcation, in the presence of synaptic noise ($D = 0.06$). Circles (○) identify the Type II model and plus signs (+) are used for Type I.

as a function of $I - I_c$ and $(I - I_c)/I_c$. We recall that the bifurcation values are $I_c = 0.183$ and 0.083 respectively for Type II and Type I models.

We first consider the case where the synaptic noise is zero. The results are shown in Fig. 15. It is seen that the coding fraction is significant for both models, but over different ranges of bias current. The Type I model is also seen to achieve slightly higher coding fractions. The range of inputs over which the Type I model encodes, i.e. its dynamic range, is smaller than for Type II, although the gap between the two models is smaller when using the relative distance to threshold. One also observes that the range of encoding for Type II is mostly below the bifurcation, while it straddles the bifurcation more for Type I.

We next compare the coding fractions for both models in the presence of a synaptic noise of fixed intensity. A noise intensity of $D = 0.06$ was used for these simulations, which corresponds to the maximum of the coding fraction in the subthreshold case (Fig. 13). We find that the maximum coding fraction for both models (peak values) are very similar, although they do not appear at the same distance from their respective bifurcations. The interval for which the coding fraction is high is larger and flatter for Type II, and further away from the bifurcation. The difference between the two models is however again smaller when the relative distance scale is used.

The performance of both types of coders was strikingly similar, indicating a minor influence of the onset mechanism for the limit cycle on the coding quality, at least in these Morris-Lecar implementations. Nevertheless we do observe the following differences. In both the subthreshold and suprathreshold case, Type I has a larger coding fraction (by about 10%) than Type II in the low noise region. However, at larger noise, we found Type II to code slightly better (again by about 10%) despite the fact that it has a slightly lower sampling rate, as shown in Fig. 17. This plot shows in fact that, although in our calibration both models have approximately the same P value (defined without RAM's), the firing rate of Type I was slightly higher than that of Type II when RAM's are present.

6. Discussion

We have studied the transduction of stimuli in the form of amplitude modulations of a periodic carrier wave. This was done for standard Type I and Type II implementations of the Morris-Lecar model. We have shown
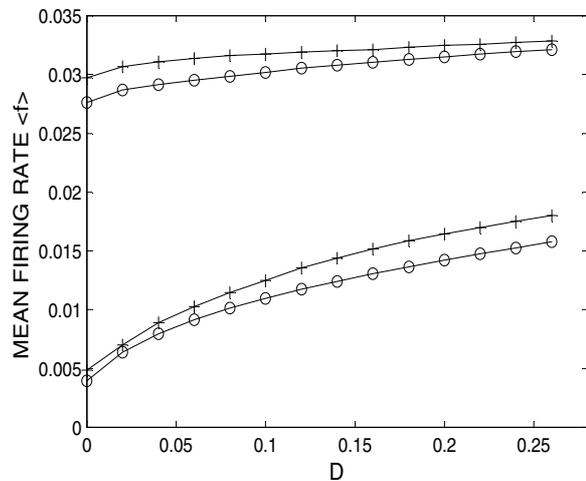

Figure 17. Mean firing rate vs. internal "synaptic" noise intensity in the presence of a random amplitude modulation of the EOD. Circles ($\circ$) identify the Type II model and plus signs ($+$) are used for Type I. Curves on top are for the suprathreshold regime while those at lower frequency are for the subthreshold regime. Current values are the same as in Fig. 9.

that this model can easily be made to exhibit the characteristic phase locking patterns seen in many neurons that respond to amplitude-modulated carrier signals, such as P-type electroreceptors and auditory neurons: the spikes always occur near a preferred phase of the carrier, but are separated by a random number of cycles of the carrier wave.

For both the Type I and II cases, such skipping patterns can be seen without amplitude modulations, and in both the subthreshold and suprathreshold regimes, as long as noise, such as synaptic noise, is also driving the dynamics. Otherwise, the dynamics always settle onto a periodic phase locked pattern. In the presence of AM's, both models can also generate skipping patterns with and even without noise; the transients caused by the ongoing stimulus are then responsible for the skipping.

However, experimental data clearly shows that skipping occurs in the absence of AM's, thus strongly suggesting the presence of noise in the internal dynamics of the receptors. As this noise is presumably not extinguished by the AM, it is appropriate to include it, both without and with bandlimited AM's. This is why we have taken care of incorporating it all along in our analysis of the coding properties. One assumption related to this point is that the intensity of the noise was kept constant for a given simulation, i.e. it did not

follow the AM in any way (it is however scaled by the mean EOD amplitude r_0, which is not changed by the AM in our study). One may want to relax this assumption in future studies since synaptic noise is likely to track the AM.

We have shown that in both Type II and Type I models, noise of synaptic origin may increase the quality of signal transduction in the subthreshold regime, especially near the threshold. Our model assumes for simplicity that this noise is additive, even though in reality such noise comes in through fluctuating conductances which multiply the voltage variable, and is thus multiplicative. Low-to-moderate noise intensities raise the firing rate of the model, allowing a better sampling of the stimulus, thus reducing reconstruction noise and increasing the coding fraction. This result is a manifestation of stochastic resonance (Gammaitoni et al., 1998) in the Morris-Lecar model in the context where the signal is an amplitude modulation of a carrier. In the suprathreshold case however, noise was found to always reduce the quality of encoding.

Because there are a large number of parameters to control, any comparison of coding capabilities in two different neuron models relies on certain strategies. Our comparison of these capabilities in the Type I and II models was based foremost on a calibration of the parameters such that the models had qualitatively and even quantitatively very similar behaviors of their firing rates across the range of AM's considered. This choice was dictated by the fact that coding quality depends strongly on firing rate. The comparison was made for two parameter sets, one producing (deterministically) a Hopf bifurcation (Type II membrane) and the other a saddle-node bifurcation (Type I membrane) to periodic firing as the bias current was increased. The amplitude and frequency of the carrier as well as the bandwidth of the Gaussian stimulus were kept the same for both models, and comparisons were made for equal intensities of internal noise.

It is not surprising that any two sets of parameters differing by the value of only one parameter such as bias or internal noise intensity yield different coding qualities (as measured by the coding fraction in our study). In this sense we have learned that it is more meaningful to characterize and compare whole curves of coding fractions across one parameter space dimension for both model types. In this picture, we can see that the qualitative behavior of the two model types is the same with respect to (1) interval histograms (Figs. 5 and 8), (2) firing rate versus internal noise (Figs. 10 and 11), (3) coding fraction versus internal noise (Figs. 13 and 14), and (4) coding fraction versus absolute and relative distance to threshold (Figs. 15 and 16); and for cases (1)–(3), this holds true in both the subthreshold and suprathreshold regimes. With our calibration, both models can exhibit very similar maximal coding fractions, even though these maxima occur at different distances to threshold.

It appears that the Type II model actually encodes better below the threshold to periodic firing in comparison to the Type I model. Our simulations suggest that this is the case because of the relative inflexibility of its firing frequency above threshold, in turn related to the resonant properties of Type II membranes (as seen in its radically different tuning curve in comparison to the Type I model—see Figs. 6 and 9).

The effect of resonance on amplitude modulation transduction is two-fold. We expect the resonance to increase information transfer as it increases the effective amplitude of the AM. On the other hand, a resonant model tends to fire at the frequency of its limit cycle, thus lowering its coding quality, especially in the vicinity and above threshold. Our study reveals that good coding is nevertheless possible for a Type II model. Future studies should in fact perform a coding comparison not only for different contrasts of the Gaussian AM stimulus ("stimulus amplitude"), but also for different carrier frequencies. Given the resonant feature of the Type II model, it is expected that its coding fraction will depend more sensitively than Type I on which carrier frequency is used, since magnification of this carrier by the resonance will magnify the AM as well. This has been found in the coding of AM's by the (Type II) Fitzhugh-Nagumo model (Longtin and St-Hilaire, 2000).

By varying only the carrier frequency, the Type I and II coding fractions may become closer or diverge from one another. This will depend on the dynamic range of the model (which is related among other things to the span of its devil's staircase; see Figs. 4 and 7). For example, bringing the EOD closer to the resonance of the Morris-Lecar Type II model will magnify the amplitude fluctuations, but more saturation (and thus worse coding) may ensue. An instructive comparison of coding across a range of carrier frequencies would have to carefully take into account how the mean firing rates vary, e.g. by redoing a match of firing rates in the sub and suprathreshold regimes as done here. This is beyond the scope of our study, but would certainly be a worthwhile endeavor. Also, we have used bandlimited

Gaussian white noise for the RAM, given our experimental motivations; its cutoff frequency is well below the intrinsic resonance frequency of the Type II model (by a factor of ten). So the effect of the resonance in the Type II model is not likely to be visible in the coding quality unless we used amplitude modulations of higher frequency.

The Type II model is found here to encode over a slightly larger range of biases than the Type I model. This is most likely due to the slower increase of the devil's staircase for the Type II model (compared to Type I) for the parameters we have chosen. At the bottom and top of the staircase, coding is not possible due to the thresold and saturation of the firing rate, respectively. The dynamic range of inputs where coding can occur lies along the staircase, or more precisely, along the slightly modified staircase due to the presence of synaptic noise and the random AM's. For our parameters, this dynamic range is smaller for Type I than Type II (compare Fig. 7 and Fig. 4, respectively), and accordingly, the range of biases where the coding fraction is significant is smaller as well for Type I. This effect is perhaps compensated by the fact that the Type II tends to fire near its resonant frequency, a property that should degrade coding of continually varying stimuli. The combination of the two effects may thus produce similar coding capabilities for both Types for the parameters we have chosen.

It is clear that coding differences depend on the particular nonlinear response of both Morris-Lecar models to sinusoidal input, as revealed e.g. in the devil's staircase and the tuning curves. What is perhaps more surprising is the similar coding quality for both models, in both subthreshold and suprathreshold regimes. This is likely a general consequence of the fact that the internal synaptic noise, as well as the on-going transients induced by the AM's, cause a linearization of the firing rate versus input bias characteristic, which improves the tracking of the stimulus by the output firing rate (this property has been discussed for Type II neurons in Chialvo et al., 1997). In fact, for the Type II case, noise and transients not only linearize the f-I curve, but also render it smooth in the first place.

The V-shaped tuning curve for the Type II model is qualitatively similar to another class of units in weakly electric fish, the so-called T-units which fire once per cycle of the carrier. In another study we have shown how noise on a Type II system can turn its tuning curve into that characteristic of a Type I system (Longtin, 2000). The fact that the V-shaped curve opens up to resemble more the tuning curve of a Type I neuron is another reason why the Type I and II models studied here have similar encoding capabilities.

Although we have focussed specifically on the coding of amplitude modulations, it is clear that a certain amount of coding may occur via phase information as well. This is expected particularly at high stimulus frequencies, where the precise placement of spikes on the cycles of the carrier can better reflect the fluctuations of the stimulus. It is known for example that phase jitter limits the encoding of high frequency amplitude modulations, and thus that phase information is important when the stimulus contains higher frequencies, even though these may still be lower than the carrier frequency. And in the electrosensory system, there are primary receptors that specialize in phase information (the aforementioned T-units). This analysis of phase coding is currently under investigation.

Finally, it would be instructive to repeat the calculations in the absence of a carrier, i.e. to focus solely on the encoding of a Gaussian bandlimited stimulus added directly to the current balance equation. That problem might be simpler since one does not have to contend with the frequency and amplitude of the carrier, and how they affect the phase locking responses of the model. One may also consider other parameter sets for which the Type I and II dynamics are better separated, both without and with synaptic noise, as measured e.g. by the shape of the phase resetting curves (Jan Benda, private communication). Eventually the effect of synaptic reversal potentials on the encoding should be considered. And a more unbiased estimate of information transfer, such as the mutual information, could also be used to uncover other differences between the coding properties of Type I and II neurons.

Acknowledgment

References

Bastian J (1981) Electrolocation 1. How the electroreceptors of Apteronotus Leptorynchus code for moving objects and other external stimuli. J. Comp. Physiol. 144: 465–479.

Bastian J (1994) Electrosensory organisms. Physics Today 47: 30–37.

Carr CE (1993) Processing of temporal information in the brain. Annu. Rev. Neurosci. 16: 223–243.

Carr CE, Friedman MA (1999) Evolution of time coding systems. Neural Comp. 11: 1–20.

Chacron MJ, Longtin A, St-Hilaire M, Maler L (2000) Suprathreshold stochastic firing dynamics with memory in P-type electroreceptors. Phys. Rev. Lett. 85: 1576–1579.

Chacron MJ, Longtin A, Maler L (2001) Negative interspike interval correlations increase the neuronal capacity for encoding time-dependent stimuli. J. Neurosci. 21: 5328–5343.

Chacron MJ, Pakdaman K, Longtin A (2003) Interspike interval correlations, phase locking and chaotic dynamics in a leaky integrate-and-fire model with dynamic threshold. Neural Comput. (in press).

Chialvo DR, Longtin A, Muller-Gerkin J (1997) Stochastic resonance in models of neuronal ensembles. Phys. Rev. E 55: 1798–1808.

Ermentrout GB (1996) Type I membranes, phase resetting curves and synchrony. Neural Comp. 8: 979–1001.

Fox RF, Gatland IR, Roy R, Vemuri G (1988) Fast, accurate algorithm for numerical simulation of exponentially correlated colored noise. Phys. Rev. A 38: 5938–5940.

French AS, Holden AV, Stein RB (1972) The estimation of the frequency response function of a mechanoreceptor. Kybernetik 11: 15–23.

Gabbiani F (1996a) Coding of time-varying signals in spike trains of linear and half-wave rectifying neurons. Network Comp. Neural Syst. 7: 61–85.

Gabbiani F, Koch C (1996b) Coding of time-varying signal in spike trains of integrate-and-fire neurons with random threshold. Neural Comput. 8: 44–66.

Gabbiani F, Koch C (2000) Principles of spike train analysis. In: Koch C, Segev I, eds. Methods in Neuronal Modeling, 2nd edn. MIT Press, Cambridge, pp. 313–360. Algorithms available at http://glab.bcm.tmc.edu/signal_processing_techniques/signal_proc.html.

Gammaitoni L, Hanggi P, Marchesoni F, Jung P (1998) Stochastic resonance. Rev. Mod. Phys. 70: 223–288.

Geisler CD, Goldberg JM (1966) A stochastic model of the repetitive activity of neurons. Biophys. J. 7: 53–69.

Gutkin BS, Ermentrout GB (1998) Dynamics of membrane excitability determine interspike interval variability: A link between spike generation mechanisms and cortical spike train statistics. Neural Comput. 10: 1047–1065.

Hodgkin AL (1948) The local electric changes associated with repetitive action in a non-medullated axon. J. Physiol. (London) 107: 165–181.

Izhikevich EM (2001) Resonate-and-fire neurons. Neural Networks 14: 883–894.

Keener JP, Hoppensteadt FC, Rinzel J (1981) Integrate and fire models of nerve membrane response to oscillatory input. SIAM J. Appl. Math. 41: 127–144.

Knight B (1972) Dynamics of encoding in a population of neurons. J. Gen. Physiol. 59: 734–766.

Longtin A (2002) Phase locking and resonances in stochastic excitable systems. Fluct. and Noise Lett. 2: 183–211.

Longtin A (2000) Effect of noise on the tuning properties of excitable systems. Chaos, Solit. and Fract. 11: 1835–1848.

Longtin A (1995) Mechanisms of stochastic phase locking. Chaos 5: 209–215.

Longtin A, St-Hilaire M (2000) Encoding carrier amplitude modulations via stochastic phase synchronization. Intern. J. Bifurc. Chaos 10: 2447–2463.

Machens CK, Stemmler MB, Prinz P, Krahe R, Ronacher B, Herz AVM (2001) Representation of acoustic communication signals by insect auditory receptor neurons. J. Neurosci. 21: 3215–3227.

Masuda N, Aihara K (2002) Spatiotemporal spike encoding of a continuous external signal. Neural Comput. 14: 1599–1628.

Morris C, Lecar H (1981) Voltage oscillations in the barnacle giant muscle fiber. Biophys. J. 35: 193–213.

Morse RP, Evans EF (1996) Enhancement of vowel coding for cochlear implants by addition of noise. Nature Med. 2: 928–932.

Nelson ME, Xu Z, Payne JR (1997) Characterization and modeling of P-type electrosensory afferent responses to amplitude modulations in a wave-type electric fish. J. Comp. Physiol. A 181: 532–544.

Press WH, Teukolski SA, Vetterling WT, Flannery BP (1992) Numerical Recipes in C: The Art of Scientific Computing, 2nd edn. Cambridge University Press, Cambridge.

Rinzel J, Ermentrout B (1991) Analysis of neural excitability and oscillations. In: Koch C, Segev I, eds. Methods in Neuronal Modeling. MIT Press, Cambridge, pp. 135–169.

Rose J, Brugge J, Anderson D, Hind J (1967) Phase-locked response to low frequency tones in single auditory nerve fibers of the squirrel monkey. J. Neurophysiol. 30: 769.

Scheich H, Bullock T, Hamstra Jr, RH (1973) Coding properties of two classes of afferent nerve fibers: High frequency receptors in the electric fish Eigenmannia. J. Neurophysiol. 36: 39–60.

St-Hilaire M (2002) M.Sc. Thesis, Physics Dept., University of Ottawa.

Strogatz SH (1994) Nonlinear Dynamics and Chaos With Applications in Physics, Biology, Chemistry and Engineering. Addison-Wesley, Reading, Mass.

Talbot W, Darian-Smith I, Kornhuber H, Mountcastle V (1968) The sense of flutter-vibration: Comparison of the human capacity with response patterns of mechanoreceptive afferents for the monkey hand. J. Neurophysiol. 31: 301.

Tsodyks MV, Markram H (1997) The neural code between neocortical pyramidal neurons depends on neurotransmitter release probability. Proc. Natl. Acad. Sci. USA: 719–723.

Turner RW, Maler L, Burrows M (1999) Electroreception and electrocommunication. J. Exp. Biol. 202 (special issue).

Wessel R, Koch C, Gabbiani F (1996) Coding of time-varying electric field amplitude modulations in a wave-type electric fish. J. Neurophysiol. 75: 2280–2293.

Xu Z, Payne JR, Nelson ME (1996) Logarithmic time course of sensory adaptation in electrosensory afferent nerve fibers in a weakly electric fish. J. Neurophysiol. 76: 13.

Zador A (1998) Impact of synaptic unreliability on the information transmitted by spiking neurons. J. Neurophysiol. 79: 1219–1229.

Zakon HH (1986) The electroreceptive periphery. In: Bullock TH, Heilingenberg W, eds. Electroreception. John Wiley and Sons, New York, pp. 103–156.